

Disorder driven splitting of the conductance peak at the Dirac point in graphene

L. Schweitzer¹ and P. Markoš²

¹*Physikalisch-Technische Bundesanstalt (PTB), Bundesallee 100, 38116 Braunschweig, Germany*

²*Department of Physics, FEI STU, 812 99 Bratislava, Slovakia*

The electronic properties of a bricklayer model, which shares the same topology as the hexagonal lattice of graphene, is investigated numerically. We study the influence of random magnetic field disorder in addition to a strong perpendicular magnetic field. We find a disorder driven splitting of the longitudinal conductance peak within the narrow lowest Landau band near the Dirac point. The energy splitting follows a relation which is proportional to the square root of the magnetic field and linear in the disorder strength. We calculate the scale invariant peaks of the two-terminal conductance and obtain the critical exponents as well as the multifractal properties of the chiral and quantum Hall states. We find approximate values $\nu \approx 2.5$ for the quantum Hall states, but $\nu = 0.33 \pm 0.1$ for the divergence of the correlation length of the chiral state at $E = 0$ in the presence of a strong magnetic field. Within the central $n = 0$ Landau band, the multifractal properties of both the chiral and the split quantum Hall states are the same, showing a parabolic $f(\alpha(s))$ distribution with $\alpha(0) = 2.27 \pm 0.02$. In the absence of the constant magnetic field, the chiral critical state is determined by $\alpha(0) = 2.14 \pm 0.02$.

PACS numbers: 73.23.-b, 71.30.+h, 73.22.-f

I. INTRODUCTION

The nature of the current carrying states near the charge-neutral Dirac point in graphene is of exceptional interest and of substantial importance for the understanding of the electrical transport properties in strong magnetic fields. The experimental observation of quantum Hall plateaus^{1,2,3,4,5,6} with $\sigma_{xy} = (2N + 1)2e^2/h$, $N = 0, 1, \dots$ strikingly emphasizes the significance of disorder, which influences the single sheet of carbon atoms forming the hexagonal lattice of graphene. Due to the two valleys appearing in the band structure, each Landau band contributes two times $2e^2/h$ to the Hall-conductivity σ_{xy} , whereas the factor of 2 accounts for the spin degeneracy.

In the absence of a magnetic field, simple on-site (diagonal) disorder gives rise to strong Anderson localization, which causes the electrical current to vanish at zero temperatures.^{7,8} This is, however, in conflict with experimental observations^{1,2,3,6,9} demonstrating that either a different type of disorder is present in real samples or that electron-electron interaction renders the one-particle picture obsolete. A disorder type being able to account for a finite conductance, is the ripple-disorder^{9,10} which is believed^{11,12} to create similar effects as originating from fluctuations of the hopping terms due to elastic strains of the intrinsic curvatures of the graphene sheet. It is also well known that the inter-valley scattering depends crucially on the type of the disorder.^{13,14,15,16,17}

Recently, a splitting of the conductivity maximum within the central Landau band at the Dirac point has been observed in high mobility graphene samples for very strong magnetic flux densities $B > 20$ T.^{3,5,6,18} The measured energy splitting $\Delta E \propto \sqrt{B}$ has been suggested⁶ to be due to a lifting of the sub-lattice symmetry caused by electron-electron interaction. Also, the effect of counter-propagating chiral edge states¹⁸, electron-lattice effects¹⁹

as well as valley ferromagnetism^{20,21,22,23,24} have been put forward to account for the observed splitting near the Dirac point. Although the proposed approaches contain many new and interesting physics based on interaction effects, we would like to retain the non-interacting particle picture in the present work and investigate the influence of a random magnetic field (RMF) which causes similar effects as ripple-disorder.^{11,12} Recently, the influence of real random hopping terms has already been studied and a splitting of the extended state in the $n = 0$ Landau band has been reported²⁵. However, the experimentally observed extremely narrow Landau band^{3,5,6,18} at the Dirac point suggests the origin of the Landau level broadening to be ripple-disorder or an equivalent disorder that also preserves the chiral symmetry.²⁶

By the use of a microscopic bricklayer model, which is topologically equivalent^{27,28} to a hexagonal lattice, and assuming a random magnetic flux disorder by introducing complex phases into the hopping terms of a tight binding Hamiltonian, we find a narrow density of states peak at the Dirac point and a splitting of the central conductance peak similar to what has been observed in experiments. We calculate the density of states, the two-terminal conductance, and the critical eigenstates, from which the respective energy and magnetic field dependence of the energy splitting, the scaling of the conductance, and the multifractal properties of the critical eigenstates are obtained. The splitting ΔE increases linearly with the strength of the random flux amplitude and shows a \sqrt{B} dependence as observed in experiments. Besides the split quantum Hall conductance peak, we find a central chiral state at $E = 0$. The latter exhibits a critical exponent $\nu = 0.33 \pm 0.1$, which determines the divergence of the localization length $\xi/\xi_0 = |E|^{-\nu}$, whereas the remaining two split bands of the central Landau level belong to the ordinary quantum Hall symmetry class with a critical exponent $\nu \approx 2.5$. The calculated multifractal proper-

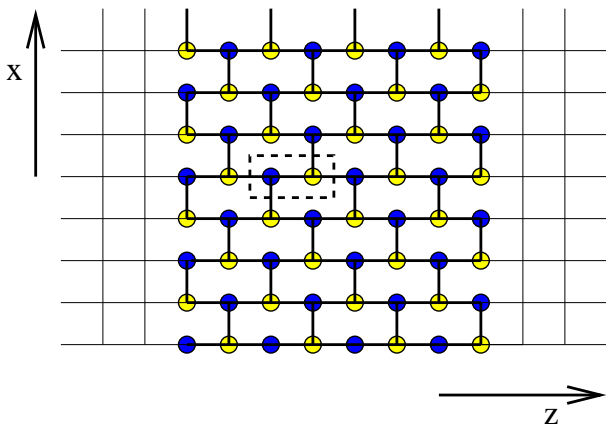


FIG. 1: (Color online) The two-dimensional bricklayer lattice which shares the same topology as the hexagonal lattice of graphene. The bi-atomic unit cell is indicated by the dashed rectangle. For the calculation of the conductance, the sample is connected to two semi-infinite leads (thin lines) with square lattice topology, and periodic boundary conditions are applied in the vertical direction (top vertical lines are connected to sites in the lowest horizontal line).

ties turn out to depend on the static magnetic field. For $B = 0$, we find $\alpha(0) = 2.14$ for the chiral state at the Dirac point. This value changes to the usual quantum Hall result $\alpha(0) = 2.27$ in the presence of a spatially constant magnetic field.

II. BRICKLAYER MODEL AND TRANSFER MATRIX METHOD

Graphene can be represented by a tight binding Hamiltonian defined on a two dimensional honeycomb lattice. In our numerical calculations, the honeycomb lattice is transformed into a bricklayer lattice as shown in Fig. 1. Each site is connected by three bonds with its nearest neighbors and has the same topology as the hexagonal lattice.^{27,28} For investigations of the spectral properties, the differences in bond length and bond angle do not matter. In other cases the length scale has to be properly adjusted, e.g., for the plaquette size $2a^2$ (bricklayer) and $(3\sqrt{3}/2)a^2$ (hexagonal lattice) where a is the respective nearest neighbor distance.

A magnetic field perpendicular to the xz -plane creates a magnetic flux through each individual plaquette,

$$\Phi_{x,z} = \frac{p}{q}h/e + \phi_{x,z} \quad (1)$$

where p and q are integers which are mutual prime, and $\phi_{x,z}$ is the random flux component. The latter is assumed to be due to ripples and to the buckling of the non-planar carbon mono-layer which causes the magnetic flux to fluctuate from plaquette to plaquette. Since the plaquette size on the bricklayer system is twice that of the square lattice, the magnetic flux density is $B = p/q \times h/(e2a^2)$.

We choose $\phi_{x,z}$ to be uniformly distributed according to $-f/2 \leq \phi_{x,z}/(h/e) \leq f/2$ so that the mean value $\langle \phi_{x,z} \rangle$ is zero and the variance is $f^2/12$. The parameter f measures the strength of the disorder with a maximal value $f = 1$.

The corresponding tight binding Hamiltonian, with spinless fermionic particle creation (c^\dagger) and annihilation (c) operators, on the bricklayer is

$$\mathcal{H} = V \sum'_{x,z} e^{i\theta_{x,z}} c_{x,z}^\dagger c_{x+a,z} + e^{-i\theta_{x-a,z}} c_{x,z}^\dagger c_{x-a,z} + V \sum_{x,z} c_{x,z}^\dagger c_{x,z+a} + c_{x,z}^\dagger c_{x,z-a}. \quad (2)$$

The complex phase factors along the vertical bonds of a given plaquette are determined by the respective flux, $\theta_{x,z+2a} - \theta_{x,z} = 2\pi\Phi_{x,z}$. We fix the length scale by $a = 1$ and set $V = 1$, which defines the energy scale. Please note that the first sum \sum' in Eq. (2) contains only the non-zero vertical hopping terms as shown in Fig. 1. An important property of the random flux model is that its disorder does not destroy the chiral symmetry of the system at the band center $E = 0$.^{29,30,31,32} Thus, the Hamiltonian (2) enables us to study both the chiral and the quantum Hall critical regimes within the same model.

For the calculation of the conductance, the samples are attached to two semi-infinite leads, which are constructed by a two-dimensional square lattice. No magnetic field is considered within the two leads. Periodic boundary conditions are assumed in the vertical (x) direction in order to eliminate surface effects and edge states in the quantum Hall regime. This requires the number of sites in the vertical direction to be even, and a multiple of $2q$.

The two-terminal conductance is calculated by the well known transfer matrix method³³

$$g = \text{Tr } t^\dagger t = \sum_i^{N_{\text{ch}}} \frac{1}{\cosh^2(\epsilon_i/2)}, \quad (3)$$

where N_{ch} is the number of open channels, t is the transmission matrix, and the ϵ_i parameterize its eigenvalues. Statistical ensembles of typically $N_{\text{stat}} = 10^4$ samples were collected and the mean value of the conductance was calculated for each set of parameters ($E, L, f, p/q$). The transformation of the honeycomb lattice into the bricklayer changes the length scale along the propagation direction, which is due to the rectangular shape of the unit cell. For computational efficiency, we still consider $L \times L$ bricklayer lattices. We verified that for different shapes, the conductance scales like $g_c \sim L_x/L_z$ at all critical points. Hence the conductance results we show are always by a factor of two larger. Therefore, it is easy to correct for our special aspect ratio when comparing with conductance results obtained by other researchers.

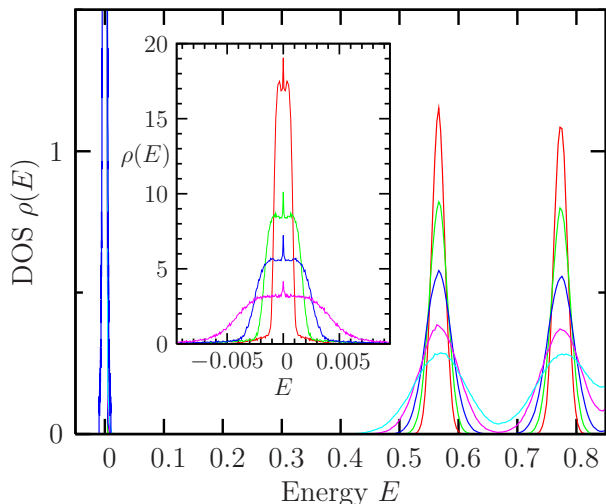


FIG. 2: (Color online) The density of states for $L \times L$ brick-layer samples with size $L = 128$, averaged over 500 disorder realizations, showing three Landau bands closest to the Dirac point for energy $E \gtrsim 0$. The random flux disorder strengths are $f = 0.001, 0.002, 0.005, 0.007$, and 0.015 , and $p/q = 1/32$. The inset shows the broadening of the narrow central Landau band together with the chiral state at $E = 0$ for $f = 0.001, 0.002, 0.003$, and 0.005 .

III. RESULTS AND DISCUSSION

A. Density of states

The density of states $\rho(E)$ was calculated by counting the eigenvalues obtained from diagonalization of $L^2 = 128 \times 128$ samples with periodic boundary conditions in both directions, averaged over 500 disorder realizations. Without disorder, $\rho(E)$ was checked to be identical with the result of a true honeycomb lattice. Fig. 2 shows $\rho(E)$ for $p/q = 1/32$ flux quantum and several disorder strengths $f = 0.001, 0.002, 0.003$, and 0.005 . Due to the symmetry around $E = 0$, the density of states is shown only for energies $E \gtrsim 0$. The Landau spectrum and the broadening of the bands is visible. However, compared with the $n = 1$ and $n = 2$ Landau bands, the central $n = 0$ one remains very narrow and is hardly discernible. Therefore, in the inset, the broadening of the narrow central band is shown in more detail where also the chiral peak at $E = 0$ is distinguishable in the middle of the broadened Landau band. A real splitting of the $n = 0$ Landau band becomes apparent only for very small disorder strength f . The total width at half height of the central band (neglecting the narrow chiral peak) is proportional to $\sqrt{p/q}f$. It should be noted that the degeneracy of the $n = 0$ Landau level found in the Dirac-model even in the presence of a random magnetic field,³⁴ is already lifted in our clean lattice model due to Harper's broadening.³⁵ In the case $B = 0$, this lattice effect also causes deviations from the linear energy dispersion away from the Dirac point.

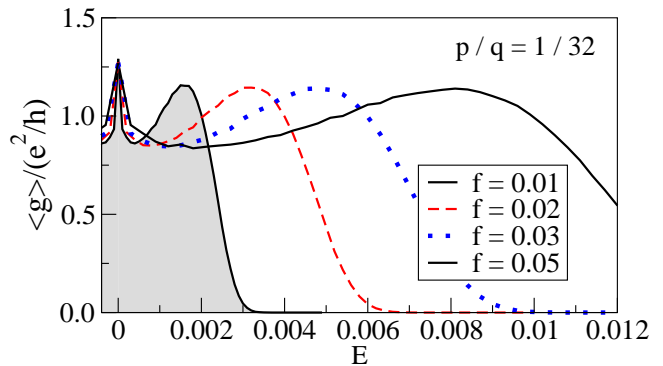


FIG. 3: (Color online) The energy dependence of the disorder averaged two-terminal conductance $\langle g(E) \rangle$ for $E \geq 0$, $p/q = 1/32$, and various random flux disorder strengths f . The size of the square samples is $L = 128$. Besides the conductance peak of the chiral state, which remains at $E = 0$, the shift of the split quantum Hall state with disorder is depicted.

Since the number of eigenvalues is the same for each principle band shown in Fig. 2, the two split $n = 0$ subbands must contain less eigenvalues than the higher Landau bands, due to the additional chiral states close to the Dirac point $E = 0$.

B. Conductance peak splitting

The energy dependence of the disorder averaged two-terminal conductance is shown in Fig. 3 for different random magnetic field disorder strengths f . Again, only the positive energies are shown, because the conductance is an even function of the energy E . With increasing f , the conductance peaks corresponding to the $n = 0$ Landau level, with peak value of about $1.12 e^2/h$, move away from $E = 0$, where the conductance peak of the scale independent chiral state remains fixed at $g(E = 0) = 1.27 e^2/h$. The disorder induced splitting ΔE of the $n = 0$ Landau level is plotted in Fig. 4 versus f for various magnetic fields with $p/q = 1/24, 1/32, 1/64$, and $1/128$. For not too large f , the data points follow the straight solid lines which are given by the relation

$$\Delta E = \sqrt{\frac{p}{q}} f. \quad (4)$$

Therefore, the conductance peak splitting shows a \sqrt{B} behavior as observed in experiments and increases linearly with the strength f of the random magnetic flux disorder. Neither a splitting nor any shift of the conductance peak due to the disorder f investigated could be observed for the $n = 1$ Landau band and $L \leq 256$.

As known from experiment,³⁶ the minimum conductivity at the Dirac point depends verifiably on disorder. Therefore, in Figure 5 we show the disorder dependence of the critical chiral conductance $\langle g(E = 0, f) \rangle$ for different magnetic fields. The two values $4/\pi (e^2/h)$

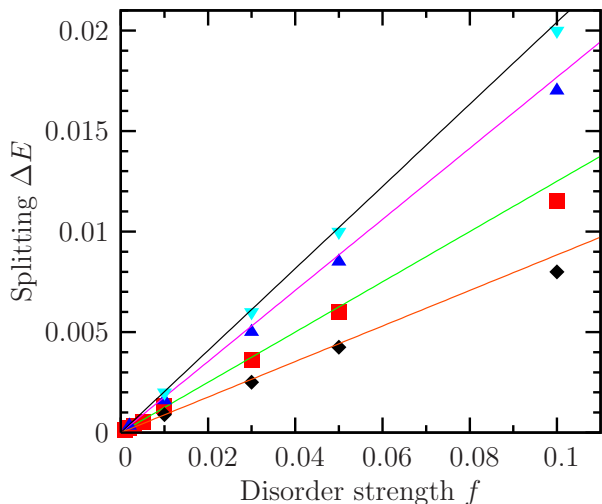


FIG. 4: (Color online) The splitting of the conducting states from the $n = 0$ Landau band obtained from the two-terminal conductance of $L = 256$ square samples versus random magnetic field disorder strength f . The magnetic field is $p/q = 1/24$ (\blacktriangledown), $p/q = 1/32$ (\blacktriangle), $p/q = 1/64$ (\blacksquare), and $p/q = 1/128$ (\blacklozenge), respectively. The straight lines follow $\Delta E = \sqrt{p/q}f$.

and $8/\pi(e^2/h)$ are indicated by solid horizontal lines. The conductance turns out to be scale invariant for sufficiently strong random flux disorder. In the limit of $f \rightarrow 1.0$, $\langle g(E = 0) \rangle$ converges to a common value which is a little larger than $8/\pi(e^2/h)$, independent of magnetic field. In contrast, a magnetic field dependence is seen for small f . In the range $0.001 < f < 0.4$, the conductance seems to approach a value somewhat smaller than $4/\pi(e^2/h)$ for all magnetic fields $p/q < 1/32$ studied. For small disorder, e.g., $f = 0.1$, and $B = 0$, the conductance scales with the sample size. A convergence to a value $\approx 4/\pi(e^2/h)$ as in the finite B case is compatible with our data.

In a finite clean system, $\langle g(E = 0, f = 0) \rangle$ is zero for $B = 0$, but increases with the system size for finite B . The former behavior is due to the vanishing density of states at $E = 0$ in the absence of a magnetic field. In the thermodynamic limit, the result for the conductance seems to depend on the order of limits $L \rightarrow \infty$ and $f \rightarrow 0$. A special case appears in the clean limit if L_z is a multiple of 3. $\langle g(E = 0, f = 0) \rangle$ turns out to be $2e^2/h$ due to the four eigenstates appearing at $E = 0$ for $k_z = \pi/3$, where $k_z = N\pi/L_z$ and $N = 1, 2, \dots$. This agrees well with the experimentally observed minimal conductivity $\sigma_{\min} = 4e^2/h$ if the electron spin is taken into account.

C. Critical Quantum Hall regime

The energetic position of the split conductance peak within the $n = 0$ Landau band as shown in Fig. 3 was estimated from the energy and size dependence of the conductance peak. For all values of disorder strength f ,

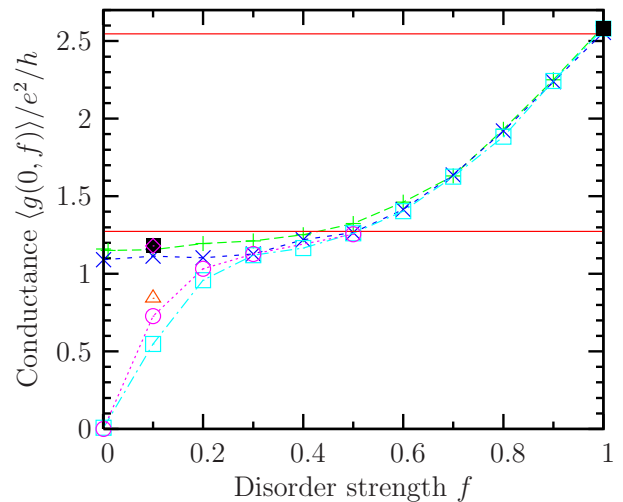


FIG. 5: (Color online) The averaged two-terminal conductance $\langle g(E = 0, f) \rangle$ for several magnetic fields (given by the ratio p/q) versus random magnetic field disorder strength f . $p/q = 1/64$: $L = 256$ ($+$), $L = 512$ (\diamond), $L = 896$ (\blacksquare). $p/q = 1/128$: $L = 256$ (\times). $B = 0$: $L = 256$ (\square), $L = 512$ (\circ), and $L = 896$ (\triangle). The horizontal lines mark the conductance values $4/\pi(e^2/h)$ and $8/\pi(e^2/h)$, respectively.

the conductance $g(E)$ exhibits a maximum around the critical energy $E_c(f)$. The maximal value of the conductance is $g_c \approx 1.12 e^2/h$. If we take into account the factor of two due to the special aspect ratio, this value is in agreement with the critical conductance $g_c = 0.6 e^2/h$ found on the square lattice with spatial correlated diagonal disorder.³⁷ Likewise, it compares well with the results $g_c = 2/\pi e^2/h$ obtained within a self-consistent Born approximation by Shon and Ando³⁸ for a graphene sheet in the presence of short or long-range scattering potentials. Finally, our result for the split conductance peak agrees also with the analytical calculations of Ostrovsky and co-workers.^{13,15,16}

A more detailed analysis of the size and energy dependence of the conductance shows that $g(E)$ exhibits a pronounced maximum around the disorder dependent critical energy $E_c(f)$. This renders the estimation of the corresponding critical exponent possible. The peak $g(E, f)$ becomes narrower when the size L of the system increases. Following the scaling theory of localization, the conductance is assumed to be a function of only one parameter in the vicinity of the critical point, $\langle g \rangle = F(L/\xi(E))$, with a diverging correlation length $\xi(E) \propto |E - E_c|^{-\nu}$. Then, we can extract the critical value of the conductance and the critical exponent assuming that

$$\langle g \rangle = g_c - A(L) [E - E_c]^2. \quad (5)$$

and

$$A(L) \propto L^{2/\nu}. \quad (6)$$

Fig. 6 shows the size and energy dependence of the conductance peak for disorder $f = 0.1$. We obtained a crit-

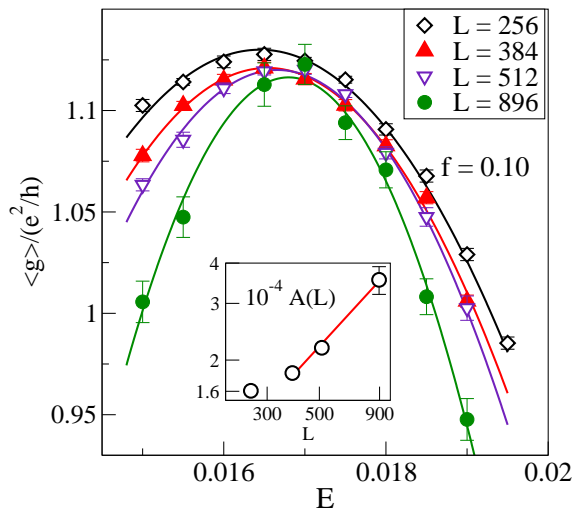


FIG. 6: (Color online) The energy dependence of the averaged conductance (g) for $p/q = 1/32$ and $f = 0.10$ calculated for the bricklayer model of size $L \times L$. Solid lines are quadratic fits, given by Eq. (5). A scaling analysis provides us with a critical exponent $\nu \approx 2.5$ if only data for $L \geq 384$ were used. The inset shows a double-logarithmic plot of the size dependence of $A(L)$ defined in (5). The solid line is a power-law fit of (6) with $\nu \approx 2.5$.

ical exponent $\nu \approx 2.5$ when only data for $L \geq 384$ were used in the scaling analysis. We observed a similar behavior for smaller disorder strength $f = 0.01$. In view of the uncertainties, we consider this to be consistent with the well known results $\nu = 2.3$ for ordinary quantum Hall systems supporting the view of the universality of the continuous quantum Hall phase transition.

The two-terminal conductance for the $n = 1$ Landau band is shown in Fig. 7 versus energy. The peak value is about $1.87 e^2/h$. The maximal available size of the system ($L = 512$) is still insufficient for a more accurate estimation of the critical parameters. Therefore, we can neither give any limiting value nor address the Landau level dependence of the critical conductance. The very slow L -dependence of the conductance in the critical region, indicating a larger localization length than for the $n = 0$ case, makes the scaling analysis and estimation of critical exponent impossible.

D. Critical chiral state

From the energy and size dependence of the mean conductance in the vicinity of the chiral critical point we extract the critical conductance, $g_c = \lim_{L \rightarrow \infty} \langle g(E = 0, L) \rangle$. Our data for the mean conductance $\langle g \rangle$ at the band center $E = 0$ exhibit a convergence to the size independent limit g_c ,

$$\langle g(E = 0, L) \rangle = g_c + b/L. \quad (7)$$

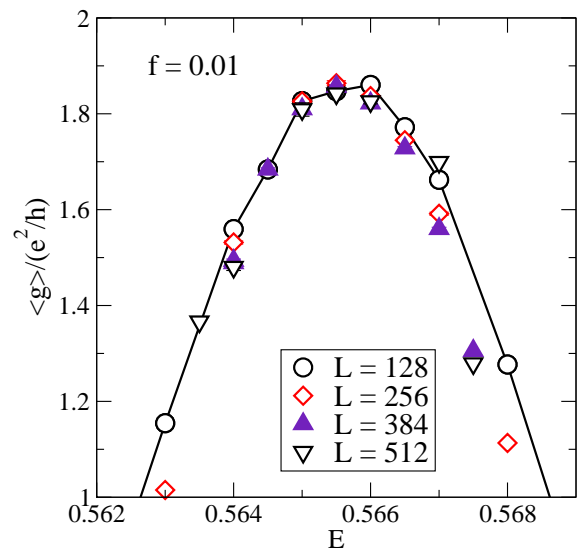


FIG. 7: (Color online) The disorder averaged two-terminal conductance versus energy in the $n = 1$ Landau band for various system sizes $L = 128, 256, 384,$ and 512 . The magnetic field is $p/q = 1/32$ and the disorder strength $f = 0.01$.

As shown in the inset of Fig. 8, $g_c \simeq 1.267 e^2/h$. This perfectly agrees with the theoretically predicted value $4/\pi e^2/h = 1.273 e^2/h$ for the spin-degenerate situation.^{13,15,16} We mention again that in our case the factor of two originates not from the spin, but from the special aspect ratio used.

To estimate the conductance fluctuations, we calculated the probability distribution $p(g)$ which proved to be Gaussian, confirming the presence of mesoscopic fluctuations also at the chiral critical point. The variance $\text{var } g = \langle g^2 \rangle - \langle g \rangle^2$ varies slightly as a function of B and f . For instance, we find $\text{var } g \approx 0.23 (e^2/h)^2$ for the data shown in Fig. 8, but $0.21 (e^2/h)^2$ for the $B = 0$ case (Fig. 9).

To analyze the critical behavior of the conductance in the vicinity of the band center, we calculated $\langle g \rangle$ for square samples of size $L = 64, 128, 192, 256,$ and 384 , within the narrow energy interval $10^{-9} \leq E \leq 10^{-4}$. Our data confirm that, after finite size correction (7), the mean conductance is a function of one parameter only, $\langle g(E, L) \rangle = G(EL^{1/\nu})$. Following scaling theory, ν is the critical exponent that governs the divergence of the correlation length, $\xi(E) \propto |E|^{-\nu}$. A more detailed analysis shows that

$$G(x) = g_c - c_0 \ln(1 + c_1 x + c_2 x^2), \quad (8)$$

with $c_0 = 0.05$, $c_1 = -0.02944$, and $c_2 = 0.02134$. Scaling analysis provides us with the critical exponent $\nu = 0.33 \pm 0.1$. Although the best scaling is obtained for $\nu = 0.33$ (as shown in Fig. 8), a reasonable scaling is also possible for values of the critical exponent in the range $0.25 < \nu < 0.45$. Again, only numerical data for much larger systems would reduce this inaccuracy.

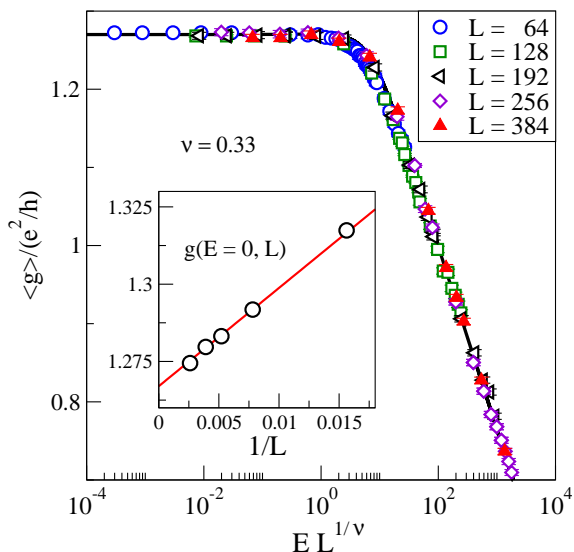


FIG. 8: (Color online) Scaling of the averaged chiral conductance in the vicinity of the critical Dirac point $E = 0$. The magnetic field is $p/q = 1/32$ and the disorder strength $f = 0.01$. The data show scaling with a critical exponent $\nu = 0.33 \pm 0.1$. The solid line is the fitted function (8). The inset shows the finite size correction $g(E = 0, L)/(e^2/h) = 1.267 + 3.178/L$, and $\text{var } g \approx 0.23 (e^2/h)^2$.

We have carefully checked that our estimate of ν is insensitive to the range of the energy interval selected. Also, we tried to compensate for the observed divergence of the critical density of states near $E = 0$, which, however, changed our estimates only marginally. We mention that our result does not satisfy the Harris criterion,³⁹ which states that $d\nu - 2 \geq 0$. There are similar results also for other models^{40,41,42,43,44,45} with chiral critical exponents $\nu < 1$.

In the absence of a constant magnetic field, we observed that the value of the conductance at $E = 0$ depends considerably on the size of the system, $g(L) = 2.62 - 11.48/L$. Even worse, the scaling behavior is fulfilled only in a very narrow interval of conductance values. From Fig. 9 we see that the width of the scaling interval is comparable with the uncertainty in the conductance due to the finite size effects. It is therefore no surprise that the estimation of the critical exponent is much more difficult. Taking into account these restrictions, we conclude that the estimated value of the critical exponent $\nu \approx 0.42$ is still in reasonable agreement with the previously obtained values $\nu = 0.35$ and $\nu = 0.42$ for a normal square lattice.^{44,45}

E. Multifractal eigenstates

The critical eigenfunctions $\psi_E(r)$ of bricklayer samples with sizes up to $L^2 = 384 \times 384$ were obtained numerically using a Lanczos algorithm. For eigenvalues close to $E = 0$, the chiral eigenstates show the expected sub-lattice

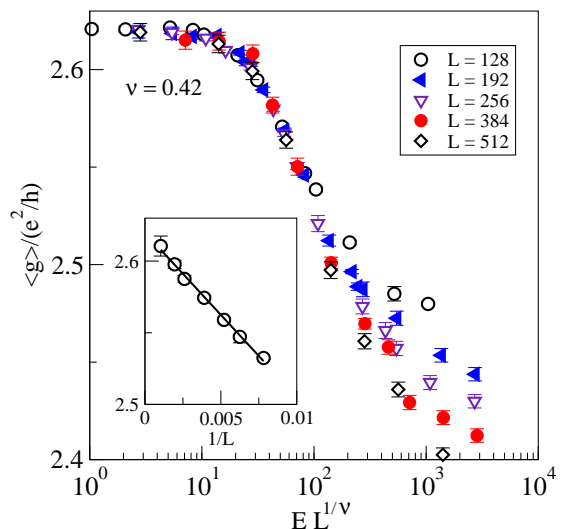


FIG. 9: (Color online) Attempt to scale the averaged conductance data close to the chiral critical point for a bricklayer system with zero homogeneous magnetic field and randomness $f = 1.0$. Bricklayer square samples of size $L = 128, 192, 256, 384$, and 512 are considered. We obtain a critical exponent $\nu = 0.42$. The inset shows the size dependence of $g(E = 0)$ for $128 \leq L \leq 960$. The solid line is $g(L)/(e^2/h) = 2.62 - 11.48/L$, and $\text{var } g \approx 0.21 (e^2/h)^2$.

polarization, since for a clean system the wavefunctions are non-zero only on one of the sub-lattices.^{25,46} This sublattice polarization is still observable in the presence of both the fluctuating random flux and the constant perpendicular magnetic field. We also notice some weak quasi one-dimensional structures making the appearance of $|\psi_{E=0}(r)|^2$ look slightly anisotropic.

A similar behavior is found for the $n = 0$ critical quantum Hall states, too. This is shown in Fig. 10 where the squared amplitude of a characteristic eigenstate with energy $E = 0.016815$ is displayed for a $L = 320$ sample with $p/q = 1/32$ and RMF strength $f = 0.1$. A closer inspection reveals an approximate sub-lattice polarization also in this case. This effect appears to be stronger than in the diagonal disordered situation.⁴⁶

The multifractal analysis was carried out as usual by utilizing the well known box counting method where the scaling of a 'box-probability' is calculated, $P(s, \lambda) = \sum_i^{N(l)} (\sum_{r \in \Omega_i(l)} |\psi_E(r)|^2)^s \sim \lambda^{\tau(s)}$, from which the generalized fractal dimensions $D(s) = \tau(s)/(s - 1)$ or, by a Legendre transform, the so called $f(\alpha(s))$ -distribution can be derived.^{47,48} Here, $\Omega_i(l)$ is the i -th box of size $l = \lambda L$ from which the s -th moment of the modulus of the normalized eigenstate $\psi_E(r)$ is taken.

In Fig. 11 we show the $f(\alpha(s))$ -distribution of two $d = 2$ chiral eigenstates at $E \approx 0$ in comparison with the parabolic approximation, $f(\alpha(s)) = d - (\alpha(s) - \alpha(0))^2 / (4(\alpha(0) - d))$, which for finite systems is normally valid only for small $|s|$. We find a value $\alpha(0) = 2.14 \pm 0.02$ when averaged over several critical chiral states in the

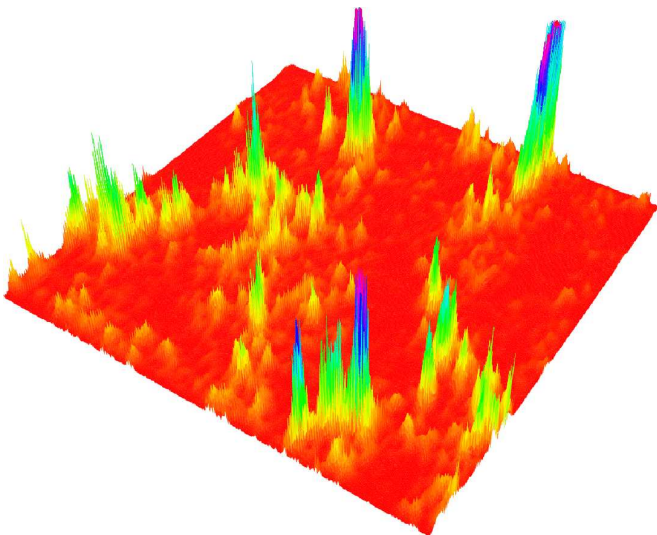


FIG. 10: (Color online) The probability density of a characteristic critical quantum Hall eigenstate of the $n = 0$ Landau band at $E = 0.016815$. The system size is $L = 320$, constant magnetic field $p/q = 1/32$, and random magnetic field strength $f = 0.1$.

case $B = 0$. This value turns out to be close to the one obtained previously for a square lattice with correlated random magnetic field.⁴⁹ For finite B , we find an averaged $\alpha(0) = 2.27 \pm 0.02$ which is the same as the $\alpha(0)$ -value of the $n = 0$ quantum Hall states. This result also agrees with $\alpha(0)$ -values published for various quantum Hall models in the range $2.26 < \alpha(0) \leq 2.29$.^{50,51,52,53} For the $n = 1$ quantum Hall state the achievable system sizes were not sufficient for the calculation of a conclusive multifractal spectrum.

We finally mention that we also checked the $E = 2.9725$ critical eigenstates within the Landau band closest to the tight-binding band edge in the presence of diagonal disorder. These outer states do not belong to the Dirac fermion sequence to be found only in the energy range $-1.0 \leq E \leq 1.0$. Again, we obtained the ordinary quantum Hall multifractality with $\alpha(0) \simeq 2.29$ and a critical conductance $g_c \simeq 1.0 e^2/h$ (including the aspect ratio factor 2).

IV. CONCLUSIONS

We investigated numerically a two-dimensional brick-layer lattice model, which shares the same topology as graphene's hexagonal lattice, in the presence of both a homogeneous and a spatially fluctuating random magnetic field. We calculated the one-particle density of states, the two-terminal conductance, and the multifractal properties of critical eigenstates. Within the very narrow $n = 0$ Landau band, we found a splitting of the two-terminal conductance peak into three sub-peaks. A central chiral conductance peak located at

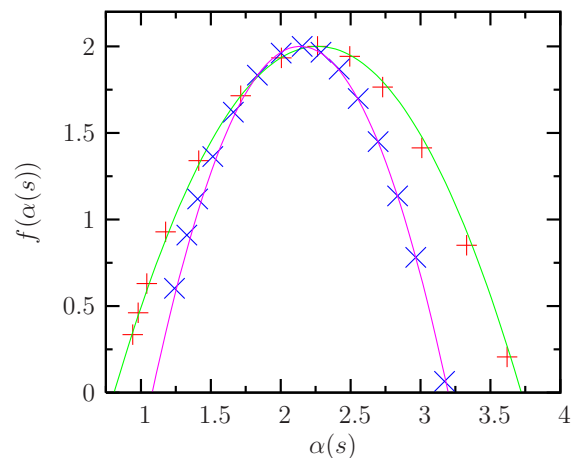


FIG. 11: (Color online) The $f(\alpha(s))$ distributions for two chiral eigenstates with energy close to $E = 0$. The parabolas are determined by the values $\alpha(0) = 2.14$ in the case of $B = 0$, $f = 1.0$ (\times), and $\alpha(0) = 2.265$ for $p/q = 1/32$, $f = 0.5$ ($+$), respectively. In both cases, the system size is $L = 320$. The data points correspond to $s = \pm 4.0, \pm 3.0, \pm 2.5, \pm 2.0, \pm 1.5, \pm 1.0, \pm 0.5$, and 0.0 .

the Dirac point $E = 0$ with a scale independent value $4/\pi e^2/h \lesssim g_c(E = 0, f) \lesssim 8/\pi e^2/h$ (including the aspect ratio factor 2), and depending on the strength of the random magnetic field f . The symmetric splitting of the two other peaks $\Delta E(p/q, f)$ increases with the square root of the applied perpendicular magnetic field expressed by the rational number p/q times a flux quantum h/e per plaquette, and linearly with the amplitude of the random magnetic flux disorder f . The scale independent conductance peak value of these critical quantum Hall states is $g_c \approx 1.12 e^2/h$ (including the aspect ratio factor 2), independent of disorder strength and applied magnetic field. The splitting of the $n = 0$ conductance peak allows for a Hall-plateau with both $\sigma_{xy} = 0$ and $\sigma_{xx} = 0$, except at $E = 0$, where the longitudinal conductance is finite due to the chiral critical state.

A similar scenario, a splitting of the Landau band and an additional central critical state with a $(\ln(|E|))^2$ singularity in the density of state was previously reported for a two state Landau model by Minakuchi and Hikami⁵⁴. They found divergences of the localization length with an exponent $\nu = 0.26$ for the central state, which is not far away from our result for the chiral critical state, and for the split Landau band $\nu = 3.1$, which is somewhat larger, but still believed by these authors to be compatible with the conventional quantum Hall universality class. Presumably, the large value has to be attributed to finite-size effects.

Our analysis of the critical eigenstates revealed the sub-lattice polarization, known from the clean system at $E = 0$, to exist at least approximately also in the random magnetic flux disordered system for energies in the vicinity of the Dirac point. Within the achieved uncertainty, the multifractal properties of the critical eigenstates in

the $n = 0$ Landau band appeared to be the same. We found the quantum Hall critical states parabolic $f(\alpha(s))$ distribution, which is determined by an $\alpha(0) = 2.27 \pm 0.02$ value, to be in accordance with the multifractal properties of the chiral critical state close to the Dirac point.

V. ACKNOWLEDGMENTS

We would like to thank Walter Apel and Ferdinand Evers for valuable discussions. PM thanks grant APVV

project No. 51-003505, VEGA project No. 2/6069/26, and PTB for hospitality.

-
- ¹ K. S. Novoselov *et al.*, Nature **438**, 197 (2005).
² Y. Zhang, Y.-W. Tan, H. L. Stormer, and P. Kim, Nature **438**, 201 (2005).
³ Y. Zhang *et al.*, Phys. Rev. Lett. **96**, 136806 (2006).
⁴ K. S. Novoselov *et al.*, Science **315**, 1379 (2007).
⁵ A. J. M. Giesbers *et al.*, Phys. Rev. Lett. **99**, 206803 (2007).
⁶ Z. Jiang, Y. Zhang, H. L. Stormer, and P. Kim, Phys. Rev. Lett. **99**, 106802 (2007).
⁷ I. L. Aleiner and K. B. Efetov, Phys. Rev. Lett. **97**, 236801 (2006).
⁸ A. Altland, Phys. Rev. Lett. **97**, 236802 (2006).
⁹ S. V. Morozov *et al.*, Phys. Rev. Lett. **97**, 016801 (2006).
¹⁰ J. C. Meyer *et al.*, Nature **446**, 60 (2007).
¹¹ A. F. Morpurgo and F. Guinea, Phys. Rev. Lett. **97**, 196804 (2006).
¹² F. Guinea, M. I. Katsnelson, and M. A. H. Vozmediano, Phys. Rev. B **77**, 075422 (2008).
¹³ P. M. Ostrovsky, I. V. Gornyi, and A. D. Mirlin, Phys. Rev. B **74**, 235443 (2006).
¹⁴ K. Nomura and A. H. MacDonald, Phys. Rev. Lett. **98**, 076602 (2007).
¹⁵ P. M. Ostrovsky, I. V. Gornyi, and A. D. Mirlin, Eur. Phys. J. Special Topics **148**, 63 (2007).
¹⁶ P. M. Ostrovsky, I. V. Gornyi, and A. D. Mirlin, Phys. Rev. Lett. **98**, 256801 (2007).
¹⁷ D. V. Khveshchenko, Eur. Phys. Lett. **82**, 57008, (2008).
¹⁸ D. A. Abanin *et al.*, Phys. Rev. Lett. **98**, 196806 (2007).
¹⁹ J.-N. Fuchs and P. Lederer, Phys. Rev. Lett. **98**, 016803 (2007).
²⁰ K. Nomura and A. H. MacDonald, Phys. Rev. Lett. **96**, 256602 (2006).
²¹ D. A. Abanin, P. A. Lee, and L. S. Levitov, Phys. Rev. Lett. **96**, 176803 (2006).
²² H. A. Fertig and L. Brey, Phys. Rev. Lett. **97**, 116805 (2006).
²³ M. O. Goerbig, R. Moessner, and B. Douçot, Phys. Rev. B **74**, 161407(R) (2006).
²⁴ J. Alicea and M. P. A. Fisher, Phys. Rev. B **74**, 075422 (2006).
²⁵ M. Koshino and T. Ando, Phys. Rev. B **75**, 033412 (2007).
²⁶ P. M. Ostrovsky, I. V. Gornyi, and A. D. Mirlin, Phys. Rev. B **77**, 195430 (2008).
²⁷ Y. Hasegawa, Y. Hatsugai, M. Kohmoto, and G. Montambaux, Phys. Rev. B **41**, 9174 (1990).
²⁸ K. Wakabayashi, M. Fujita, H. Ajiki, and M. Sgrist, Phys. Rev. B **59**, 8271 (1999).
²⁹ J. Miller and J. Wang, Phys. Rev. Lett. **76**, 1461 (1996).
³⁰ A. Furusaki, Phys. Rev. Lett. **82**, 604 (1999).
³¹ C. Mudry, P. W. Brouwer, and A. Furusaki, Phys. Rev. B **59**, 13221 (1999).
³² P. W. Brouwer, C. Mudry, B. D. Simons, and A. Altland, Phys. Rev. Lett. **81**, 862 (1998).
³³ J. B. Pendry, A. MacKinnon, and P. J. Roberts, Proc. R. Soc. Lond. A **437**, 67 (1992).
³⁴ Y. Aharonov and A. Casher, Phys. Rev. A **19**, 2461 (1979).
³⁵ P. G. Harper, Proc. Phys. Soc. (London) A **68**, 874 (1955).
³⁶ Y.-W. Tan *et al.*, Phys. Rev. Lett. **99**, 246803 (2007).
³⁷ L. Schweitzer and P. Markoš, Phys. Rev. Lett. **95**, 256805 (2005).
³⁸ N. H. Shon and T. Ando, J. Phys. Soc. Jpn. **67**, 2421 (1998).
³⁹ A. B. Harris, J. Phys. C: Solid State Phys. **7**, 1671 (1974).
⁴⁰ Y. Morita and Y. Hatsugai, Phys. Rev. B **58**, 6680 (1998).
⁴¹ V. Z. Cerovski, Phys. Rev. B **62**, 12775 (2000).
⁴² A. Eilmes, R. A. Römer, and M. Schreiber, Physica B **296**, 46 (2001).
⁴³ V. Z. Cerovski, Phys. Rev. B **64**, 161101(R) (2001).
⁴⁴ P. Markoš and L. Schweitzer, Phys. Rev. B **76**, 115318 (2007).
⁴⁵ L. Schweitzer and P. Markoš, Physica E **40**, 1335 (2008).
⁴⁶ A. L. C. Pereira and P. A. Schulz, Phys. Rev. B **77**, 075416 (2008).
⁴⁷ T. C. Halsey *et al.*, Phys. Rev. A **33**, 1141 (1986).
⁴⁸ A. Chhabra and R. V. Jensen, Phys. Rev. Lett. **62**, 1327 (1989).
⁴⁹ H. Potempa and L. Schweitzer, Ann. Phys. (Leipzig) **8**, SI-209 (1999).
⁵⁰ B. Huckestein, B. Kramer, and L. Schweitzer, Surface Science **263**, 125 (1992).
⁵¹ B. Huckestein and L. Schweitzer, Phys. Rev. Lett. **72**, 713 (1994).
⁵² R. Klesse and M. Metzler, Europhys. Lett. **32**, 229 (1995).
⁵³ F. Evers, A. Mildenberger, and A. D. Mirlin, Phys. Rev. B **64**, 241303(R) (2001).
⁵⁴ K. Minakuchi and S. Hikami, Phys. Rev. B **53**, 10898 (1996).